



Published in final edited form as:

J Neural Eng. 2016 August ; 13(4): 046016. doi:10.1088/1741-2560/13/4/046016.

SiC Protective Coating for Photovoltaic Retinal Prostheses

Xin Lei¹, Sheryl Kane², Stuart Cogan³, Henri Lorach^{4,5}, Ludwig Galambos¹, Philip Huie^{4,5}, Keith Mathieson⁶, Theodore Kamins¹, James Harris¹, and Daniel Palanker^{4,5}

¹Department of Electrical Engineering, Stanford University, Stanford, California, USA

²Work performed at EIC Laboratories, Norwood, Massachusetts, USA; now at Amgen, Cambridge, Massachusetts, USA

³University of Texas at Dallas, Richardson, Texas, USA

⁴Hansen Experimental Physics Laboratory, Stanford University, Stanford, California, USA

⁵Department of Ophthalmology, Stanford University, Stanford, California, USA

⁶Institute of Photonics, University of Strathclyde, Glasgow, Scotland, UK

Abstract

Objective—To evaluate PECVD SiC as a protective coating for retinal prostheses and other implantable devices, and to study their failure mechanisms *in vivo*.

Approach—Retinal prostheses were implanted in rats subretinally for up to 1 year. Degradation of implants was characterized by optical and scanning electron microscopy. Dissolution rates of SiC, SiN_x and thermal SiO₂ were measured in accelerated soaking tests in saline at 87°C. Defects in SiC films were revealed and analyzed by selectively removing the materials underneath those defects.

Main results—At 87°C SiN_x dissolved at 18.3±0.3nm/day, while SiO₂ grown at high temperature (1000°C) dissolved at 1.04±0.08Å/day. SiC films demonstrated the best stability, with no quantifiable change after 112 days. Defects in thin SiC films appeared primarily over complicated topography and rough surfaces.

Significance—SiC coatings demonstrating no erosion in accelerated aging test for 112 days at 87°C, equivalent to about 10 years *in vivo*, can offer effective protection of the implants. Photovoltaic retinal prostheses with PECVD SiC coatings exhibited effective protection from erosion during the 4-month follow-up *in vivo*. The optimal thickness of SiC layers is about 560nm, as defined by anti-reflective properties and by sufficient coverage to eliminate defects.

Introduction

The spectrum of implantable electro-neural interfaces for restoration and control of sensory, motor, and other brain functions is rapidly expanding. Examples include cochlear implants [1–3], deep brain stimulators [4–7], cortical motor prostheses [8–10], cortical visual prostheses [11–12] and retinal prostheses [13–17], amongst others. The majority of electrical

implants employ metal or ceramic enclosures with cable feed-throughs to protect the electronics from exposure to body fluids and associated corrosion [10,14–15,18]. This approach results in rather bulky implants and difficult surgeries that involve separate placements for the power supplies and electrode arrays, and routing of interconnecting cables.

Our group developed a silicon photodiode array implanted sub-retinally for restoration of sight to patients blinded by degenerative retinal diseases, such as age-related macular degeneration and retinitis pigmentosa [16–17]. With pulsed near-infrared light providing both power and visual information, the implant is completely wireless, greatly reducing implant size and simplifying surgery.

Since this implant is not packaged in a hermetic metal enclosure, it is exposed to body fluids. Without an optimized protective coating, the device remained functional in short-term (under 1 year) studies *in vitro* and *in vivo*, but with detectable degradation. For long-term use of integrated circuit (IC) and micro-electro-mechanical systems (MEMS)-based biomedical devices, a biocompatible encapsulation layer is necessary to provide stable protection against water and ion ingress.

Dielectric materials deposited by low-pressure chemical vapor deposition (LPCVD) at high temperatures (800–900°C) have exhibited good stability and barrier properties in long-term *in vivo* studies [19–21]. However, such temperatures are incompatible with encapsulation of ICs. Development of an encapsulation layer which can be deposited at temperatures below 400°C would be tremendously beneficial since it would allow its use for protection of ICs [22]. Low temperature (395°C) LPCVD silicon oxide (SiO₂) implanted sub-retinally in rabbits was found to dissolve after 6–12 months [23]. Polymers, such as Parylene, are used in the medical industry for encapsulation of the neural implants [24–26]. Due to its low relative permittivity, high resistivity, biocompatibility and conformal deposition, Parylene is suitable as an electrical isolation material for implantable devices. Adhesion of Parylene to inorganic substrates can be improved by adhesion promoter and thermal treatment [27]. However, Parylene has relatively high water vapor transmission rate (WVTR) compared to many dielectric materials [26,28], therefore Parylene by itself is not sufficient to protect implanted ICs. Atomic layer deposited (ALD) Al₂O₃ is conformal and hermetic, yet found to dissolve in water [26,29]. An Al₂O₃ and Parylene bilayer structure was proposed to improve its resistance to moisture and the encapsulation lifetime [26]. Diamond-like carbon (DLC) coatings [30] and ultra-nano-crystalline diamond (UNCD) coatings [31–33] have demonstrated biocompatibility, resistance to corrosion and wear, and are being used in medical implants, with some concerns regarding delamination in an aqueous environment caused by high residual stress, leakage current, pinholes near sharp corners, and a relatively high deposition temperature.

As an alternative, amorphous silicon carbide (α -SiC:H) deposited at a low temperature was proposed as a protective coating due to its availability in semiconductor processing, compatibility with IC technology, biocompatibility [34–36], contamination barrier properties [37–40] and low dissolution rate in saline, compared to other commonly used dielectric

materials for IC passivation, such as silicon nitride (SiN_x) and low-temperature SiO_2 [41–44].

In this study, we implanted retinal prosthetic devices for up to 1 year and characterized their degradation by optical and scanning electron microscopy (SEM) to assess the device failure mechanisms *in vivo*. We also measured the dissolution rates of SiC, SiN_x and thermal SiO_2 in accelerated soaking tests to compare stability of those dielectric materials. We revealed and analyzed the defects in SiC films, and defined the optimal thickness of SiC layer for reliable protection of the chronic implants.

Methods

Material deposition

SiC was deposited by plasma-enhanced chemical vapor deposition (PECVD) at EIC Laboratories, Inc. (Norwood, MA). The precursors were SiH_4 and CH_4 (1:3 ratio of SiH_4/CH_4) in an Ar carrier gas. The deposition temperature was 325°C at a pressure of 800mTorr and an RF power frequency of 13.56MHz. The SiN_x used in dissolution rate tests was deposited by PECVD at the Stanford Nanofabrication Facility (SNF) using Surface Technology Systems (STS) PECVD. The precursors were SiH_4 and NH_3 (40:33.5 ratio of SiH_4/NH_3) at a deposition temperature of 350°C and pressure of 650 mTorr. Dual frequency (13.56MHz and 187.5kHz) deposition was used. SiN_x was deposited as the top surface coating of retinal prostheses by PECVD at SNF (Plasma-Therm Shuttlelock SLR-730-PECVD). This tool used a capacitive-coupled plasma with 13.56MHz RF power. Precursors were SiH_4 and NH_3 (5:3 ratio of SiH_4/NH_3), with He and N_2 carrier gases. The deposition temperature was 350°C at a pressure of 950mTorr. SiO_2 was grown by wet thermal oxidation in a resistance-heated oxidation furnace at 1000°C .

Device fabrication

Three types of structures were used in this study. To minimize confusion, they are denoted as Type I, II and III, respectively.

Type I structures are retinal prosthetic implants fabricated at SNF using complementary metal-oxide-semiconductor (CMOS) and MEMS technologies. The fabrication process includes eight lithography steps on silicon-on-insulator (SOI) wafers with $30\mu\text{m}$ silicon device layers [45]. Each implant consists of an array of 142 hexagonal pixels, which are $70\mu\text{m}$ in width. An individual pixel contains 2 or 3 photodiodes connected in series between active and return electrodes. Photodiodes and pixels are isolated by $5\mu\text{m}$ -wide trenches filled with undoped polysilicon (Figure 1a). The implants are 1mm in diameter and $30\mu\text{m}$ thick. The main difference in the current devices from the previously described devices [45] is that the electrodes are connected to PN junctions with the opposite polarity – the active electrode connected to the p-type silicon region. This provides anodic-first pulses of current, optimal for sub-retinal stimulation [18,46]. Devices were fabricated on two wafers, both having 60nm of PECVD SiN_x (Plasma-Therm) on top of 70–80nm of thermally grown SiO_2 (thermal oxide) on the surface. One wafer has an additional 240nm layer of SiC on the top surface. The backside and sidewalls of all implants were covered with 480nm of thermally

grown SiO₂. Three Type I implants from each wafer were used in *in vivo* experiments. All of the 142 pixels of each implant were tested.

To facilitate defect analysis in SiC coatings, Type II structures were fabricated similarly to Type I devices but on bulk silicon wafers, making the total array thickness ~520μm. In addition to the 240nm thick SiC films, some of Type II arrays had thicker SiC coating ~560nm. These thick arrays were not used for *in vivo* experiments.

Type III structures are bulk silicon substrates (520μm thickness) with 5μm wide and 33μm deep trenches etched using the Bosch process (Surface Technology Systems STSetch2) at SNF. A thermal oxidation at 1000°C for 100 minutes followed the trench etching to conformally grow 480nm SiO₂ on the samples. SiC films of 560nm thickness were then deposited on the top surface of some samples, and 180nm-thick SiC films were deposited on others. Type III structures were used for the defect analysis, but not for *in vivo* experiments.

In vivo experiments

Each of the six Type I retinal prostheses (three with SiC coating and three without) were implanted sub-retinally in a different rat (six rats in total). The implantation technique was similar to the one previously reported by our group [17,47] and performed in agreement with Stanford University institutional guidelines and the Statement for the Use of Animals in Ophthalmic and Vision Research. After a period of time (from 4 months to 1 year), implants were extracted from the tissue and cleaned in an enzyme solution (Tergazyme, 1%) for one day, and then further cleaned with deionized water and isopropyl alcohol (IPA). Explanted devices were examined with optical and scanning electron microscopy. Some devices were sputter coated with a thin layer of metal (~10nm) to improve the SEM imaging by reducing the charging effects. It was not always possible to compare the same device and the same pixel before and after the implantation due to randomness of the defect locations. However, each optical and SEM image is representative of the type of implant in terms of the device structure and changes after the implantation.

Dissolution rate

Dissolution rates of dielectric materials in saline were measured in accelerated soaking tests. SiC, SiN_x, and SiO₂-coated silicon substrates (520μm thickness) were sealed in glass vials filled with saline, and placed in an oven with the temperature maintained at 87°C for up to 112 days. Samples were periodically taken out of the chamber, rinsed with deionized water, dried and analyzed. The dissolution rate study at elevated temperature was performed in a low-phosphate saline (LPS), comprised of 126mM NaCl, 5mM Na₂HPO₄, and 1.4mM NaH₂PO₄.

Five samples each of the SiC, SiN_x and SiO₂ coatings were used in the accelerated aging tests. SiC and SiN_x were grown on double-side polished silicon substrates. Before the soaking test, the thickness of SiC and SiN_x films was directly measured by selectively etching away the dielectric materials in a small region and measuring the step using surface profilometry. SiC films were 694±10nm thick on each side, and SiN_x films were 520±5nm thick on each side. SiO₂ were grown on single-side polished silicon substrates. Thickness of SiO₂ films on silicon substrates was measured using spectral reflectometry (Nanometrics

Nanospec 210XP), assuming the refractive index of SiO₂ to be 1.45 in the visible range. The five SiO₂ samples were found to be 511±3nm thick.

During the soaking tests of SiC and SiN_x, transmission-mode Fourier transform infrared spectroscopy (FTIR, Nicolet 6700) measurements were taken periodically on each sample to monitor changes of the films. The transmission FTIR spectra peaks were fitted, assuming Gaussian peak shapes, near the Si-C (~758cm⁻¹) or Si-N (~820cm⁻¹, 930cm⁻¹) stretch frequencies, and the areas under the peaks were integrated. Prior to the soaking tests, we calibrated the integrated areas of fitted Gaussian peaks measured by FTIR to the thickness measured by surface profilometry by linear regression on samples of 4 different thicknesses for both SiC and SiN_x. All subsequent FTIR peak areas were converted to film thickness using these fitted linear models. Assuming the dissolution rates on both sides of the sample exposed to the same electrolyte are the same, the dissolution rate of a single exposed surface was calculated as half of the observed dissolution rate from two surfaces. For SiO₂ films, spectral reflectometry was performed periodically during the soaking test. The dissolution rate of each film was calculated by plotting the total film thickness versus soaking time.

Defect analysis

Defect analysis was performed only on SiC films since all other coatings were gradually dissolving. To reveal the defects in the SiC films, Type II arrays were soaked in buffered oxide etch (BOE) 6:1 (volume ratio of 40% NH₄F in water to 49% HF in water) for 10 minutes to etch SiN_x and SiO₂ through any defects in the SiC films. After etching, the defects became visible under an optical microscope. Type III structures were analyzed similarly by etching materials underneath the SiC to reveal defects in the SiC films. Specifically, samples were soaked in BOE 6:1 for 7 minutes to etch SiO₂. Some samples were further etched isotropically by xenon difluoride (XeF₂) gas (Xactix e-1) to remove several microns of silicon. For cross-sectional SEM analysis of samples coated with 560nm SiC films, an additional SiO₂ etch in BOE 6:1 for 40 seconds was performed after cross sectioning the sample in order to recess the oxide and emphasize the SiC layer.

Results

Degradation of the implants in vivo

Implants without SiC coating degraded significantly during the 4-month sub-retinal implantation. SiN_x layer was completely dissolved on all pixels and devices, which was evident from the color change of the devices after implantation (Figures 1c, d compared to 1a, b). Platinum wires connecting the PN junctions to electrodes became exposed (Figure 1d). On one implant, polysilicon in the trench started to degrade (Figure 2c), while on the other implant (Figure 2b), this region did not show any visible changes (Figure 2a).

All pixels without SiC coating implanted for 1 year showed visible degradation. However, the degradation was not uniform across a device, as shown in Figure 3a; some pixels exhibit more degradation than others. In some of the trenches, polysilicon was completely dissolved, leaving a thin SiO₂ membrane covering the trench top (Figure 3b, 1). As a result, the metal wires on top of these empty trenches were mechanically compromised (Figure 3b,

2, and 3c, 2). Some thin SiO₂ films that originally covered the trench top were displaced after the polysilicon underneath was dissolved (Figure 3c, 3).

Despite the degradation, the implanted devices continued to function until they were explanted at least 7 months later [17], indicating that the SiO₂ films with metal wires on top of the empty trenches were displaced only during explantation (Figure 3). Prolonged exposure of the implants *in vivo* will eventually lead to complete dissolution of the polysilicon in the trenches, which is likely to result in the loss of mechanical support, leading to device failure. During very long *in vivo* exposure, we speculate that the 70nm of SiO₂ will eventually dissolve as well [48]. Once the active area (single-crystal silicon) of the devices is exposed to physiological environment, the silicon is expected to dissolve rapidly [43], and the devices will eventually stop functioning.

To evaluate the protective properties of SiC, three devices with 240nm of SiC coating were implanted in three different rats for 4 months. One implant did not show any visible degradation under the optical microscope (Figure 4c, d). Two other implants had minor degradation at isolated defect points, visible as small patches of color change near the middle of the polysilicon-filled trenches (Figure 4e, f, arrows) compared to the image before implantation (Figure 4a, b). These defects were seen on 51 out of 142 pixels on one device, and 41 out of 142 on another. The patches of color changes indicate the presence of defects in the SiC films near the middle of the polysilicon-filled trenches, which allowed dissolution of the underlying SiN_x.

In summary, unprotected retinal implants degrade during prolonged *in vivo* exposure, while SiC films provided effective protection of the implants.

Dissolution rates of protective coatings

Following the observation of the device degradation and dissolution of SiN_x *in vivo*, we measured the dissolution rate of SiN_x, SiC, and SiO₂ films under accelerated aging test conditions — soaking the devices in saline at 87°C.

SiN_x exhibited a highly reproducible and linear dissolution rate of 18.3±0.3nm/day (single surface) over the course of 28 days at 87°C (Figure 5a). In addition, water penetration and bubbling was visible by day 1, and color changes indicative of thinning occurred throughout the course of soaking. By day 28, white dots appeared, suggesting wafer oxidation. Overnight between days 28 and 29, the remaining silicon nitride on each sample (15–23nm per side) dissolved, and the wafers oxidized extensively. This result corresponded well with the observations *in vivo*, where SiN_x films on the retinal prostheses completely dissolved after 4 months.

In contrast, the five samples coated with SiC exhibited excellent stability. After more than 16 weeks in LPS at 87°C, they showed neither visible degradation nor quantifiable dissolution (Figure 5a). This result is in agreement with the earlier measurement of SiC dissolution rate over 28 days at 90°C [41], and explains why SiC-coated devices were much more stable *in vivo*. The measured film thickness fluctuated within ~2% (standard deviation) over the course of soaking — likely an artifact of the peak fitting procedure. Defects in the SiC films

could also contribute to variation in the measurement, if silicon under the defects oxidizes and dissolves, forming localized corrosion that could scatter light during the FTIR measurements.

Thermally grown SiO_2 dissolved very slowly but steadily at $1.04 \pm 0.08 \text{ \AA/day}$ in saline at 87°C (Figure 5b). Thus a SiO_2 coating of 70nm would last for ~ 700 days under the accelerated aging conditions, corresponding to tens of years *in vivo*. This explains why the single-crystal silicon part of the implant did not degrade *in vivo* after 1 year, with 70–80nm of SiO_2 covering it.

Defect analysis

Continuity of the protective coatings is critical for device longevity. Any defect in the film will expose the underlying materials to the harsh environment. Figure 5 demonstrates a measurable dissolution rate of SiN_x and SiO_2 , while the thickness of SiC didn't change over the course of soaking tests. Therefore, we only performed defect analysis on SiC films deposited on different structures to find weak points in these films, which may lead to degradation of the devices.

For 560nm SiC films, examination of a total area of 11 cm^2 of the top surface of Type III structures showed no defects (Figure 6a). Occasional defects were found on the sidewalls of the trenches covered with SiC (Figure 6b). The scalloping on the sidewall due to the Bosch process likely increased the defect occurrence. SiC covered the trench sidewalls and bottoms continuously to the bottom (Figure 7a, b). For 180nm SiC films, the trench sidewalls were covered by SiC only down to $\sim 4.5 \mu\text{m}$ depth (Figure 7c, e). A thin layer (tens of nanometers) of SiC covered the bottom of the trenches. Overhanging SiC films at the corners are visible (Figure 7d) and are emphasized by deliberately etching the underlying SiO_2 layer.

Similar tests on Type II arrays coated with 240nm SiC films revealed defects exclusively in the middle of the polysilicon-filled trenches (Figure 8b). This result matches well the defects observed after the 4-month *in vivo* implantation (Figure 4e, f). For samples coated with 560nm SiC, no defects were found anywhere on the structures (Figure 8d). The defect density in SiC films depended on both the device topography and the film thickness. The $5 \mu\text{m}$ -wide trenches were oxidized and filled with polysilicon for electrical isolation and mechanical support (Figure 9a). The middle of the trenches has a small seam where polysilicon grown from the sidewalls joins (indicated by the arrow in Figure 9b). The small gaps near the surface are likely to result in defects, if not adequately covered. The 240nm of SiC coating did not cover these gaps (Figure 9c), while a 560nm layer completely coated the gaps (Figure 9d). Therefore, to properly protect the steps on the surface of the device and eliminate the associated defects in the SiC films, a minimum thickness of the coating, which depends on the topography of the device, must be used. For our retinal prostheses, a SiC thickness of 560nm appears to provide sufficient protection, although this must still be confirmed pending the 1 year *in vivo* follow-up.

Discussion

Devices not coated with SiC exhibited considerable degradation after 4 months *in vivo*, as shown in Figure 2. Devices with open trenches around each pixel (Figure 2c) exhibited more erosion than the ones with filled trenches (Figure 2b). But regardless the extent of degradation, the fact that it is noticeable in all uncoated devices indicates the need for a good protective coating.

SiC films appear to protect the silicon wafers very well: we have not observed dissolution of this coating in accelerated aging, nor any defects in thick ($\sim 1\mu\text{m}$) SiC films deposited on flat surfaces. However, we observed a few defects or weak spots in 200–300nm thick SiC films in the middle of the filled trenches (Figure 8b), where the surface of the underlying polysilicon is not smooth (Figure 9c). Eliminating such seams in the trenches would improve the stability of such devices. Alternatively, using thicker SiC can completely cover these rough features, as shown in Figure 9d with 560nm coating.

Silicon is known to dissolve in saline along preferential crystallographic planes, generating rectangular or square defects [43]. Silicon also reacts actively with many biological enzymes and fluids [49,50] and degrades after interactions with cell cultures [51]. In aqueous media, SiN_x is oxidized to form SiO_2 and NH_3 , and SiO_2 hydrolyzes into $\text{Si}(\text{OH})_4$ [52–54]. Therefore, a silicon implant with SiO_2 and SiN_x coatings will not survive long enough for chronic human use. SiC is known to react with O_2 and H_2O at very high temperatures (800–1000°C) [55–57], however, it is chemically inert under physiological conditions. Except for a possible observation of SiC surface oxidation [43], no chemical reactions involving SiC under physiological conditions have been reported.

To estimate the SiC coating lifetime, we assumed an acceleration factor of $2^{T/10}$, which has been used for polymers in medical devices and other applications [58], assuming first-order rate kinetics for the dissolution process. Under this scheme, the aging factor at 87°C compared to physiological temperature (37°C) is $2^{(87-37)/10} = 2^5 = 32$, which means that a day of accelerated aging corresponds to about a month at physiological temperature. In this study, the SiC coatings did not change after 112 days at 87°C, translating to no detectable degradation for roughly 10 years under physiological conditions.

Dissolution of SiN_x coatings and polysilicon in the trenches was the primary cause of device failure in this study. Eliminating SiN_x and polysilicon should greatly increase the lifetime of the devices. SiC can not only replace SiN_x as the protective coating, but also serve as a part of the anti-reflective coating for the retinal implant, in combination with the underlying SiO_2 . Simulation by the transfer matrix method [59,60] (Figure 10) showed that 560nm of SiC on top of 310–380nm of SiO_2 could reduce reflection of 880nm light below 10% at vertical incidence. SiO_2 and SiC films of such thickness exhibit low defect densities even in areas of complex topography, and therefore can provide effective protection.

The backside of the retinal prostheses can be coated with SiC at a much lower temperature to be compatible with the sputtered iridium oxide film (SIROF) electrode used in our devices. Amorphous SiC can be deposited at 175°C by electron cyclotron resonance (ECR) PECVD [61], at <200°C by PECVD [43,62], and even at room temperature by RF

magnetron sputtering [63], although the stability of those films in saline solution needs to be investigated. Therefore, SiC coating can be deposited after SIROF deposition and release of the devices. Sidewalls of the devices can be coated with SiC by a combination of depositions from the top and bottom. Alternatively, the back and sidewalls of the implant can be coated with metal.

Aside from increasing the SiC film thickness, the defect density can be reduced by growth interruption during the SiC deposition. The defects in SiC films on the trench sidewalls can also be reduced by decreasing the scalloping related to the Bosch process used to etch trenches in the silicon. H₂ annealing at an elevated temperature has been demonstrated to smooth sidewalls [64–66].

The dissolution rate of SiC and other dielectric materials might be different with an electric field applied. Further study of the retinal prostheses *in vivo* with chronic photovoltaic activation will shed more light on this topic.

Conclusions

Significant degradation of unprotected photovoltaic retinal prostheses was found after 4-month implantation, especially in the polysilicon-filled trenches. PECVD SiC films were much more effective than SiN_x and SiO₂ coatings in protecting the devices *in vivo*. Accelerated aging tests did not change the thickness of SiC film after 112 days in saline at 87°C. The SiN_x coating was much less stable, and dissolved at 18.3±0.3nm/day at 87°C. Thermal SiO₂ grown at high temperature (1000°C) was more stable, but still dissolved very slowly at 1.04±0.08A/day at 87°C in saline. SiC films exhibited some defects on complicated topography and rough surfaces. The defect density could be reduced or eliminated by smoothening the underlying surface or by increasing the SiC film thickness. Overall, PECVD SiC films have desirable properties as protective coatings for implantable electronics. A combination of thermal SiO₂ with a PECVD SiC film should be adequate for providing anti-reflective coating and protecting retinal prostheses for long-term use.

Acknowledgments

Funding was provided by the US National Institutes of Health (grant R01-EY-018608, D.P.), the Department of Defense (grant W81XWH-15-1-0009, D.P.), and the Stanford Spectrum fund (D.P.). K.M. was supported by an SU2P fellowship as part of a RCUK Science Bridges award. H.L. was supported in part by the Fondation Voir et Entendre (Paris) and Pixium Vision. Fabrication was performed in part at the Stanford Nanofabrication Facility, which is supported by National Science Foundation through the NNIN (grant ECS-9731293). Sample preparation by SEM (FEI XL30 Sirion) was performed at the Stanford Nano Shared Facilities (SNSF). Accelerated SiC degradation testing at EIC Laboratories was performed partly by Doug Orsi and Chathuri Gunasekharan.

References

1. Crosby, PA.; Daly, CN.; Money, DK.; Patrick, JF.; Seligman, PM.; Kuzma, JA. Cochlear implant system for an auditory prosthesis. United States Patent. 4,532,930. 1985.
2. McDermott H. An advanced multiple channel cochlear implant. IEEE Trans Biomed Eng. 1989; 36:789–97. [PubMed: 2744794]
3. Wilson BS, Finley CC, Lawson DT, Wolford RD, Eddington DK, Rabinowitz WM. Better speech recognition with cochlear implants. Nature. 1991; 352:236–38. [PubMed: 1857418]

4. Benabid AL, Pollak P, Gao D, Hoffmann D, Limousin P, Gay E, Payen I, Benazzouz A. Chronic electrical stimulation of the ventralis intermedius nucleus of the thalamus as a treatment of movement disorders. *J Neurosurg.* 1996; 84:203–14. [PubMed: 8592222]
5. Limousin P, Krack P, Pollak P, Benazzouz A, Ardouin C, Hoffmann D, Benabid AL. Electrical stimulation of the subthalamic nucleus in advanced Parkinson's disease. *N Engl J Med.* 1998; 339:1105–11. [PubMed: 9770557]
6. Kumar R, Lozano AM, Kim YJ, Hutchison WD, Sime E, Halket E, Lang AE. Double-blind evaluation of subthalamic nucleus deep brain stimulation in advanced Parkinson's disease. *Neurology.* 1998; 51:850–5. [PubMed: 9748038]
7. Kupsch A, et al. Pallidal deep-brain stimulation in primary generalized or segmental dystonia. *N Engl J Med.* 2006; 355:1978–90. [PubMed: 17093249]
8. Hochberg LR, Serruya MD, Friebs GM, Mukand JA, Saleh M, Caplan AH, Branner A, Chen D, Penn RD, Donoghue JP. Neuronal ensemble control of prosthetic devices by a human with tetraplegia. *Nature.* 2006; 442:164–71. [PubMed: 16838014]
9. Hochberg LR, et al. Reach and grasp by people with tetraplegia using a neurally controlled robotic arm. *Nature.* 2012; 485:372–5. [PubMed: 22596161]
10. Shenoy KV, Sahani M, Churchland MM. Cortical control of arm movements: a dynamical systems perspective. *Annu Rev Neurosci.* 2013; 36:337–59. [PubMed: 23725001]
11. Campbell PK, Jones KE, Huber RJ, Horch KW, Normann RA. A silicon-based, three-dimensional neural interface: manufacturing processes for an intracortical electrode array. *IEEE Trans Biomed Eng.* 1991; 38:758–68. [PubMed: 1937509]
12. Normann RA, Maynard EM, Rousche PJ, Warren DJ. A neural interface for a cortical vision prosthesis. *Vision Res.* 1999; 39:2577–87. [PubMed: 10396626]
13. Zrenner E, et al. Subretinal electronic chips allow blind patients to read letters and combine them to words. *Proc Biol Sci.* 2011; 278:1489–97. [PubMed: 21047851]
14. Ahuja AK, Dorn JD, Caspi A, McMahon MJ, Dagnelie G, Dacruz L, Stanga P, Humayun MS, Greenberg RJ. Argus II Study Group. Blind subjects implanted with the Argus II retinal prosthesis are able to improve performance in a spatial-motor task. *Br J Ophthalmol.* 2011; 95:539–43. [PubMed: 20881025]
15. Humayun MS, et al. Interim results from the international trial of Second Sight's visual prosthesis. *Ophthalmology.* 2012; 119:779–88. [PubMed: 22244176]
16. Mathieson K, et al. Photovoltaic retinal prosthesis with high pixel density. *Nat Photonics.* 2012; 6:391–7. [PubMed: 23049619]
17. Lorach H, et al. Photovoltaic restoration of sight with high visual acuity. *Nat Med.* 2015; 21:476–82. [PubMed: 25915832]
18. Jensen RJ, Rizzo JF III. Thresholds for activation of rabbit retinal ganglion cells with a subretinal electrode. *Exp Eye Res.* 2006; 83:367–73. [PubMed: 16616739]
19. Anderson DJ, Najafi K, Tanghe SJ, Evans DA, Levy KL, Hetke JF, Xue XL, Zappia JJ, Wise KD. Batch-fabricated thin-film electrodes for stimulation of the central auditory system. *IEEE Trans Biomed Eng.* 1989; 36:693–704. [PubMed: 2744793]
20. Hetke JF, Lund JL, Najafi K, Wise KD, Anderson DJ. Silicon ribbon cables for chronically implantable microelectrodes arrays. *IEEE Trans Biomed Eng.* 1994; 41:314–21. [PubMed: 8063297]
21. Weiland JD, Anderson DJ. Chronic neural stimulation with thin-film, iridium oxide electrodes. *IEEE Trans Biomed Eng.* 2000; 47:911–8. [PubMed: 10916262]
22. Plummer, JD.; Deal, MD.; Griffin, PB. *Silicon VLSI Technology.* Upper Saddle River, NJ: Prentice Hall; 2000. p. 725
23. Hammerle H, Kobuch K, Kohler K, Nisch W, Sachs H, Stelzle M. Biostability of micro-photodiode arrays for subretinal implantation. *Biomaterials.* 2002; 23:797–804. [PubMed: 11771699]
24. Loeb GE, Bak MJ, Salzman M, Schmidt EM. Parylene as a chronically stable, reproducible microelectrode insulator. *IEEE Trans Biomed Eng.* 1977; 24:121–8. [PubMed: 408260]
25. Hsu JM, Rieth L, Normann RA, Tathireddy P, Solzbacher F. Encapsulation of an integrated neural interface device with Parylene C. *IEEE Trans Biomed Eng.* 2009; 56:23–9. [PubMed: 19224715]

26. Xie X, Rieth L, Williams L, Negi S, Bhandari R, Caldwell R, Sharma R, Tathireddy P, Solzbacher F. Long-term reliability of Al₂O₃ and Parylene C bilayer encapsulated Utah electrode array based neural interfaces for chronic implantation. *J Neural Eng.* 2014; 11:1–9.
27. Charnet J, Bitterli J, Sereda O, Liley M, Renaud P, Keppner H. Optimizing Parylene C adhesion for MEMS processes: potassium hydroxide wet etching. *J Microelectromech Syst.* 2013; 22:855–64.
28. Chen TN, Wu DS, Wu CC, Chiang CC, Chen YP, Horng RH. High-performance transparent barrier films of SiO_x/SiN_x stacks on flexible polymer substrates. *J Electrochem Soc.* 2006; 153(10):F244–8.
29. Potts SE, et al. Ultra-thin aluminium oxide films deposited by plasma-enhanced atomic layer deposition for corrosion protection. *J Electrochem Soc.* 2011; 158:132–8.
30. Roy RK, Lee KR. Biomedical applications of diamond-like carbon coatings: a review. *J Biomed Mater Res B Appl Biomater.* 2007; 83:72–84. [PubMed: 17285609]
31. Xiao X, Birrell J, Gerbi JE, Auciello O, Carlisle JA. Low temperature growth of ultrananocrystalline diamond. *J Appl Phys.* 2004; 96:2232–9.
32. Xiao X, et al. In vitro and in vivo evaluation of ultrananocrystalline diamond for coating of implantable retinal microchips. *J Biomed Mater Res B Appl Biomater.* 2006; 77:273–81. [PubMed: 16245292]
33. Chen YC, Tsai CY, Lee CY, Lin IN. In vitro and in vivo evaluation of ultrananocrystalline diamond as an encapsulation layer for implantable microchips. *Acta Biomater.* 2014; 10:2187–99. [PubMed: 24440422]
34. Bolz A, Amon M, Ozbek C, Heublein B, Schaldach M. Coating of cardiovascular stents with a semiconductor to improve their hemocompatibility. *Tex Heart Inst J.* 1996; 23:162–6. [PubMed: 8792547]
35. Amon M, Bolz A, Schaldach M. Improvement of stenting therapy with a silicon carbide coated tantalum stent. *J Mater Sci - Mater Med.* 1996; 7:273–8.
36. Rzany A, Schaldach M. Smart material silicon carbide: reduced activation of cells and proteins on a SiC:H-coated stainless steel. *Prog Biomed Res.* 2001; 4:182–94.
37. Chang CY, Fang YK, Huang CF, Wu BS. Novel passivation dielectrics — the boron-or phosphorus-doped hydrogenated amorphous silicon carbide films. *J Electrochem Soc.* 1985; 132:418–22.
38. Loboda, MJ.; Michael, KW. Silicon carbide metal diffusion barrier layer. United States Patent. 5,818,071. 1998.
39. Merchant, SM.; Misra, S.; Roy, PK. Silicon carbide barrier layers for porous low dielectric constant materials. United States Patent. 6,100,587. 2000.
40. Nemani, S.; Xia, LQ.; Yieh, E. Dual frequency plasma enhanced chemical vapor deposition of silicon carbide layers. United States Patent. 6,465,366 B1. 2002.
41. Cogan SF, Edell DJ, Guzelian AA, Liu YP, Edell R. Plasma-enhanced chemical vapor deposited silicon carbide as an implantable dielectric coating. *J Biomed Mater Res A.* 2003; 67:856–67. [PubMed: 14613234]
42. Maloney JM, Lipka SA, Baldwin SP. In vivo biostability of CVD silicon oxide and silicon nitride films. *Master Res Soc Symp Proc.* 2005; 872:1–6.
43. Hsu JM, Tathireddy P, Rieth L, Normann AR, Solzbachera F. Characterization of a-SiC_x:H thin films as an encapsulation material for integrated silicon based neural interface devices. *Thin Solid Films.* 2007; 516:34–41. [PubMed: 18437249]
44. Bai Q, Wise KD, Anderson DJ. A high-yield microassembly structure for three-dimensional microelectrode arrays. *IEEE Trans Biomed Eng.* 2000; 47:281–9. [PubMed: 10743769]
45. Wang L, et al. Photovoltaic retinal prosthesis: implant fabrication and performance. *J Neural Eng.* 2012; 9:1–11.
46. Boinagrov D, Pangratz-Fuehrer S, Goetz G, Palanker D. Selectivity of direct and network-mediated stimulation of the retinal ganglion cells with epi-, sub- and intraretinal electrodes. *J Neural Eng.* 2014; 11:1–11.
47. Mandel Y, et al. Cortical responses elicited by photovoltaic subretinal prostheses exhibit similarities to visually evoked potentials. *Nat Commun.* 2013; 4:1–9.

48. Ahn S, Spuhler PS, Chiari M, Cabodi M, Unlu MS. Quantification of surface etching by common buffers and implications on the accuracy of label-free biological assays. *Biosens Bioelectron.* 2012; 36:222–9. [PubMed: 22560160]
49. Birchall JD, Chappell JS. The chemistry of aluminum and silicon in relation to Alzheimers disease. *Clin Chem.* 1988; 34:265–7. [PubMed: 2830051]
50. Bayliss SC, Buckberry LD, Harris PJ, Tobin M. Nature of the silicon–animal cell interface. *J Porous Mater.* 2000; 7:191–5.
51. Sadow, SE. *Silicon Carbide Biotechnology.* Elsevier Science; 2012.
52. Osenbach JW, Knolle WR. Behavior of a-SiN:H and a-SiON:H Films in Condensed Water. *J Electrochem Soc.* 1992; 139:3346–51.
53. Vogt M, Hauptmann R. Plasma-deposited passivation layers for moisture and water protection. *Surf Coat Technol.* 1995; 74–75:676–81.
54. Schmitt G, Schultze JW, Fasbender F, Bus G, Luth H, Schoning MJ. Passivation and corrosion of microelectrode arrays. *Electrochim Acta.* 1999; 44:3865–83.
55. Munro RG, Dapkunas SJ. Corrosion characteristics of silicon carbide and silicon nitride. *J Res Natl Inst Stand Technol.* 1993; 98:607–31.
56. Kraft T, Nickel KG, Gogotsi YG. Hydrothermal degradation of chemical vapour deposited SiC fibres. *J Mater Sci.* 1998; 33:4357–64.
57. Pastila P, Helanti V, Nikkila A, Mantyla T. Environmental effects on microstructure and strength of SiC-based hot gas filters. *J Eur Ceram Soc.* 2001; 21:1261–8.
58. Hukins DW, Mahomed A, Kukureka SN. Accelerated aging for testing polymeric biomaterials and medical devices. *Med Eng Phys.* 2008; 30:1270–4. [PubMed: 18692425]
59. Knittl, Z. *Optics of Thin Films.* Wiley; London: 1976.
60. Pettersson LA, Roman LS, Inganas O. Modeling photocurrent action spectra of photovoltaic devices based on organic thin films. *J Appl Phys.* 1999; 86:487–96.
61. Loboda MJ. Low temperature PECVD growth and characterization of a-SiC:H films deposited from silacyclobutane and silane/methane precursor gases. *Springer Proceedings in Physics.* 1992; 71:271–80.
62. Jiang L, Chen X, Wang X, Xu L, Stubhan F, Merkel K. a-SiCx-H films deposited by plasma-enhanced chemical vapor deposition at low temperature used for moisture and corrosion resistant applications. *Thin Solid Films.* 1999; 352:97–101.
63. Ledermann N, Baborowski J, Muralt P, Xantopoulos N, Tellenbach JM. Sputtered silicon carbide thin films as protective coating for MEMS applications. *Surf Coat Technol.* 2000; 125:246–50.
64. Sato T, Mitsutake K, Mizushima I, Tsunashima Y. Micro-structure transformation of silicon: a newly developed transformation technology for patterning silicon surfaces using the surface migration of silicon atoms by hydrogen annealing. *Jpn J Appl Phys.* 2000; 39:5033–8.
65. Kuribayashi H, Hiruta R, Shimizu R, Sudoh K, Iwasaki H. Shape transformation of silicon trenches during hydrogen annealing. *J Vac Sci Technol A.* 2003; 21:1279–83.
66. Lee MCM, Wu MC. Thermal annealing in hydrogen for 3-D profile transformation on silicon-on-insulator and sidewall roughness reduction. *J Microelectromech Syst.* 2006; 15:338–43.

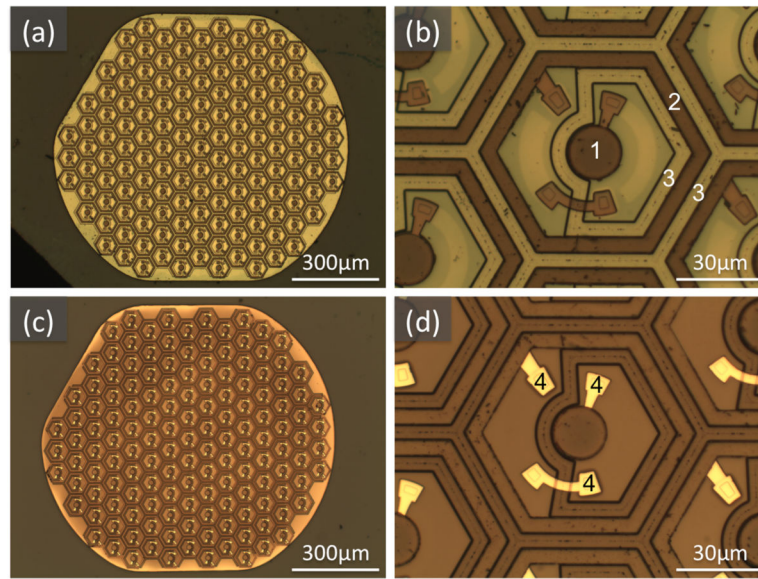


Figure 1. Optical microscopy of retinal prostheses (Type I) without SiC coating

(a) A 2-diode pixel device before implantation. (b) One pixel of the device in (a); 1 -active electrode, 2 - return electrode, 3 - trenches filled with polysilicon. (c, d) 4 months after sub-retinal implantation in a rat eye. The drastic color change and exposed metal wires (4, bright yellow) indicate the dissolution of SiN_x .

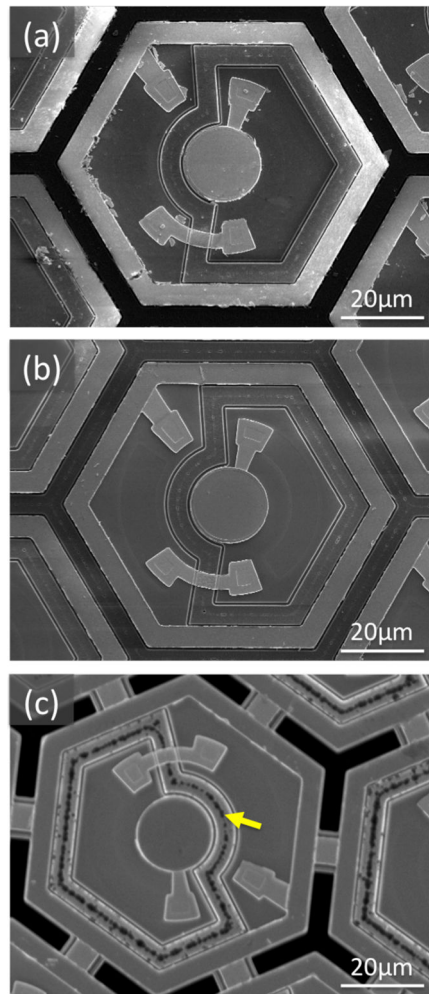


Figure 2. Scanning electron microscopy of retinal prostheses (Type I) without SiC coating
 (a) A 2-diode pixel before implantation. (b, c) 4 months after sub-retinal implantation in a rat eye. The implant in (c) exhibits degradation in the polysilicon trench region (arrow), while (b) did not show visible changes compared to (a). All implants shown in this figure are from the same wafer. Only one pixel of each implant is shown, but all pixels on an implant have similar degradation.

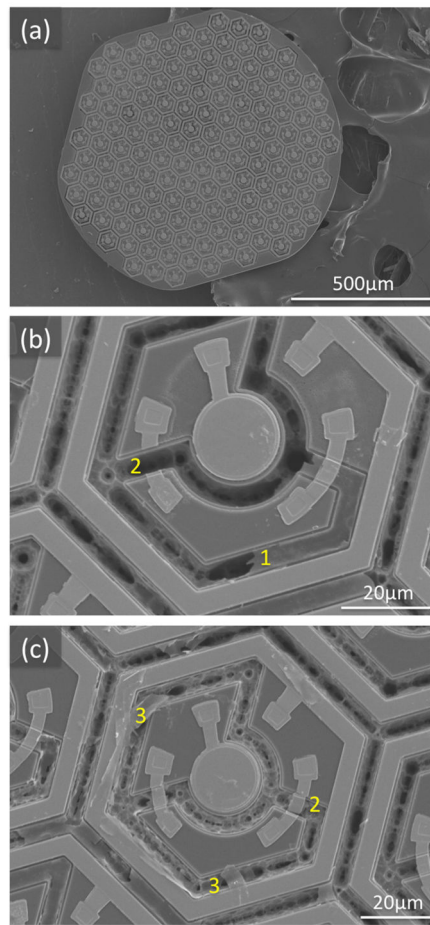


Figure 3. Scanning electron microscopy of retinal prostheses (Type I) without SiC coating after 1-year implantation

(a) All pixels in this device have visible degradation, albeit not uniform across the device. Both 3-diode pixels in (b) and (c) exhibit significant degradation. Polysilicon in some trenches is largely dissolved, leaving only a thin SiO_2 film covering the trench top (b1). Metal wires on top of the dissolved trenches could break (b2, c2). Some SiO_2 films that originally covered the trench top were displaced (c3).

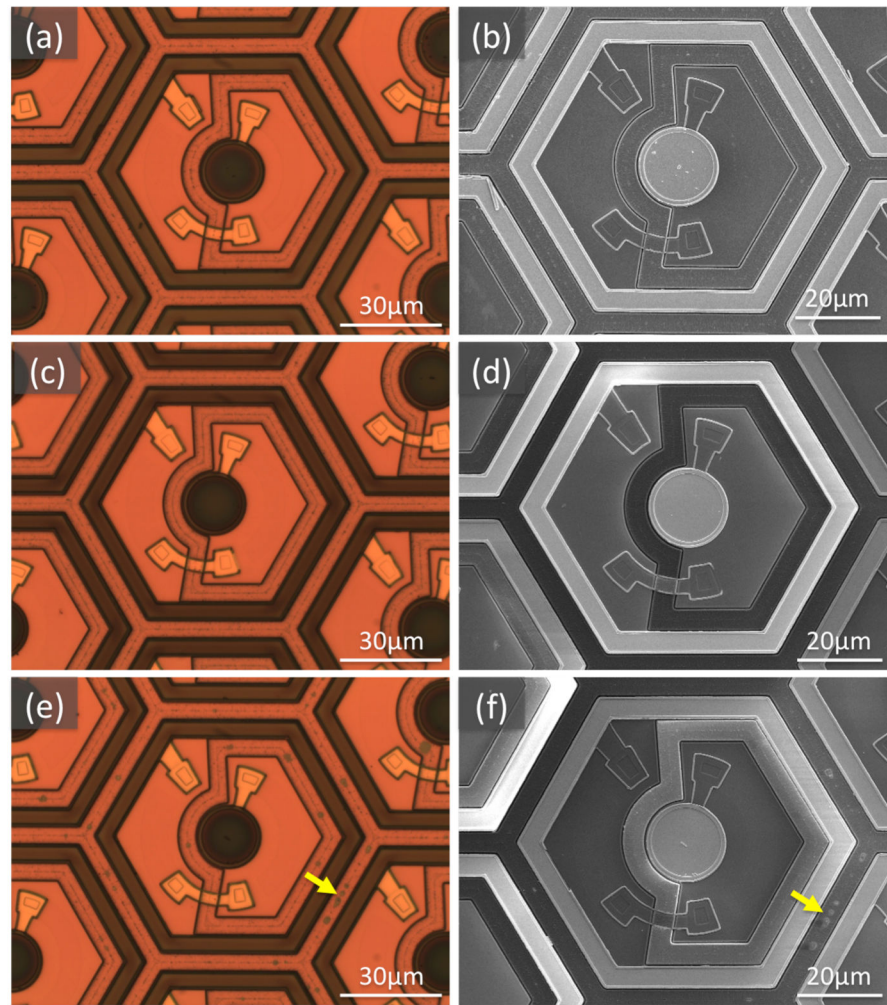


Figure 4. Retinal prostheses (Type I) with 240nm SiC coating

(a, b) A 2-diode pixel before implantation. (c–f) 4 months after sub-retinal implantation in a rat eye. (c, d) exhibits no signs of degradation, while (e, f) showed small patches of color change in the middle of the polysilicon-filled trench (arrows), indicating defects in the SiC film.

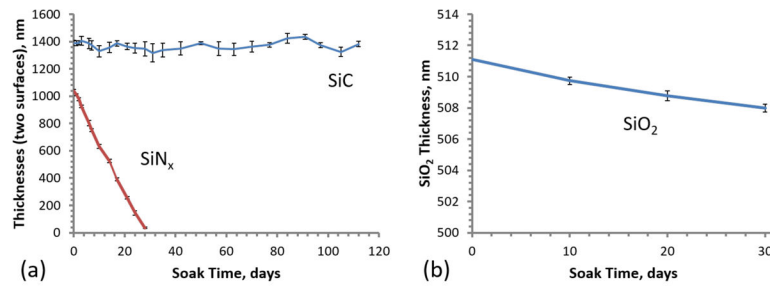


Figure 5. Dissolution rate of dielectric materials in saline at 87°C

(a) PECVD SiN_x dissolved at $18.3\text{nm}\pm0.3\text{nm/day}$, while PECVD SiC showed no quantifiable dissolution up to 112 days. (b) Thermal SiO₂ dissolved at $1.04\pm0.08\text{A/day}$ (data were normalized to the average thickness of SiO₂ on day 0).

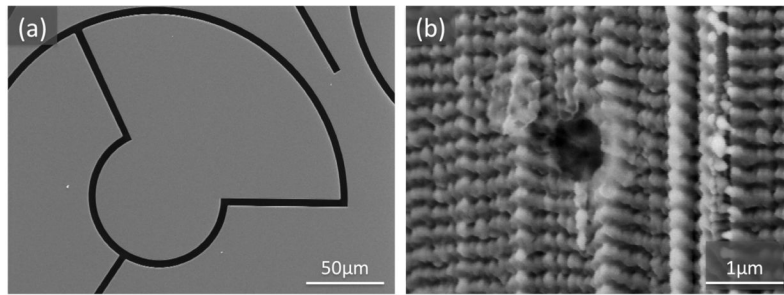


Figure 6. Defect characterization of SiC films (Type III)

(a) Top view of 560nm SiC film deposited on a smooth surface of 480nm thermal SiO₂ on a bulk Si substrate with etched and oxidized trenches. No defects were found on 11cm₂ of the top surface examined. (b) A defect on a trench sidewall.

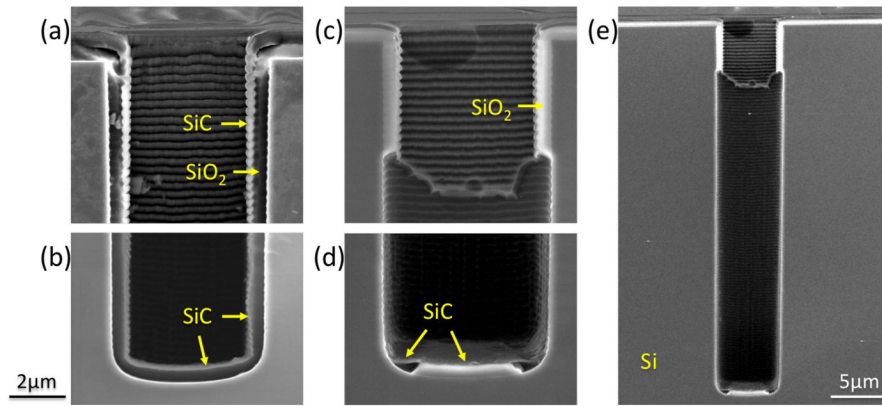


Figure 7. Trench coverage of SiC films (Type III)

(a, b) 560nm SiC deposited on 480nm SiO₂ on a bulk Si substrate with etched and oxidized trenches. The continuous SiC film on the sidewall and bottom is pointed out by the arrows.
 (c, d, e) 180nm SiC deposited on 480nm SiO₂ on Si substrate with etched and oxidized trenches. The SiC film was continuous only at the top ~4.5μm of the trench.

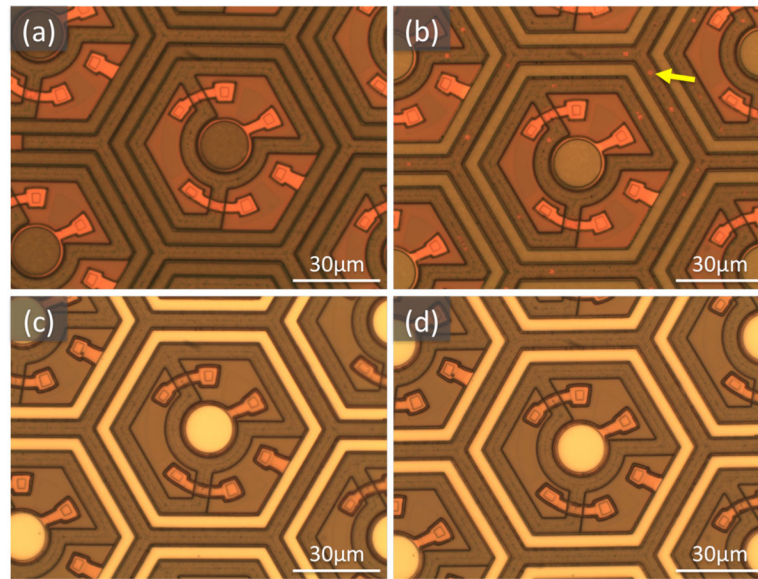


Figure 8. Defect characterization of SiC films deposited on retinal prostheses (Type II)
 (a, b) 3- diode array with 240nm of SiC. (c, d) 3-diode array with 560nm of SiC. (b, d) After etching in BOE 6:1 for 10 minutes to reveal defects in the SiC films. (b) With 240nm SiC, defects were visible in the middle of polysilicon filled trenches (arrow). (d) No defects were visible with 560nm SiC.

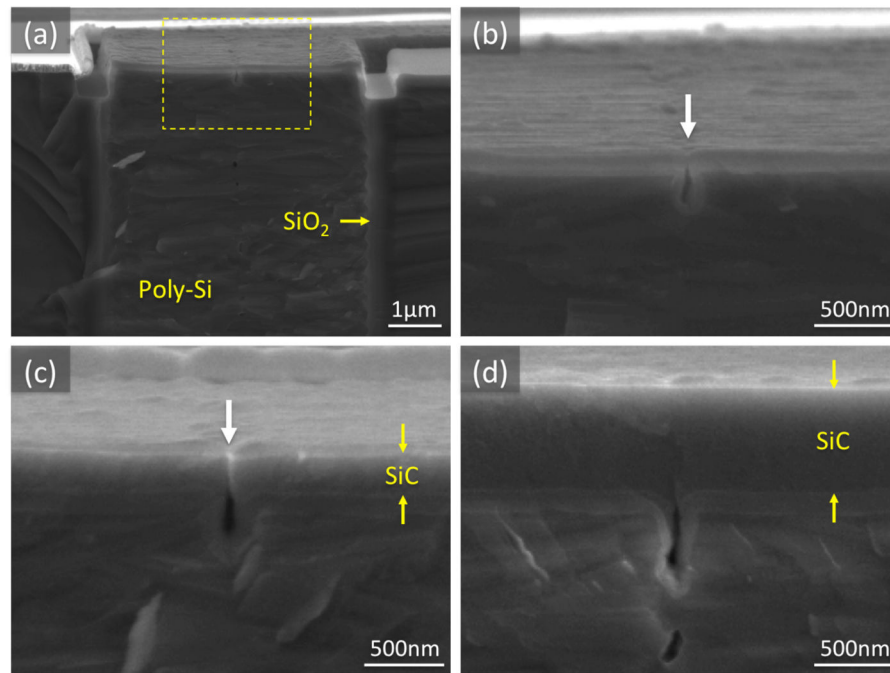


Figure 9. Cross-section of retinal prostheses (Type II) in the trench region

(a) Sample with no SiC coating, showing the top $\sim 5\mu\text{m}$ of the polysilicon-filled trench. (b) Zoom-in image of the middle of the trench (yellow dashed rectangle) of (a). White arrow points to the gap in polysilicon. (c) A sample with 240nm SiC coating. Small gap in the middle of the trench not fully covered by SiC is indicated by the white arrow. (d) Sample with 560nm SiC coating completely covering the gap.

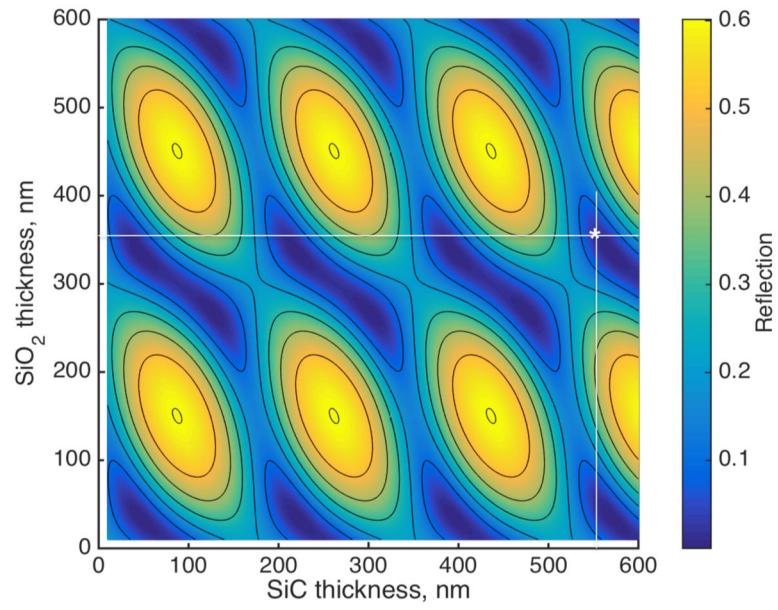


Figure 10. Calculated optical reflectivity of the SiC and thermal SiO₂ stack in saline
 560nm of SiC on top of 310–380nm of SiO₂ could reduce reflection of 880nm light below
 10% at vertical incidence.